


Article

Characterization of Hydroxyapatite/Chitosan Composite Coating Obtained from Crab Shells on Low-Modulus Ti–25Nb–8Sn Alloy through Hydrothermal Treatment

Hsueh-Chuan Hsu ¹, Shih-Ching Wu ¹, Chien-Yu Lin ² and Wen-Fu Ho ^{2,*} 

¹ Department of Dental Technology and Materials Science, Central Taiwan University of Science and Technology, Taichung 40601, Taiwan

² Department of Chemical and Materials Engineering, National University of Kaohsiung, Kaohsiung 81148, Taiwan

* Correspondence: fujii@nuk.edu.tw

Abstract: In this study, hydroxyapatite/chitosan (HA/CS) composite coatings were prepared by hydrothermal treatment on the surface of low-modulus Ti–25Nb–8Sn alloy to improve the surface bioactivity of the alloy. HA, the main mineral composition of the human skeleton, has excellent bioactivity and is often used as a surface coating on biometal implants. CS, a natural polymer with good antibacterial, hydrophilic and non-toxic characteristics, is often used as dermal regeneration templates, hemostatic agents and drug delivery systems. In this experiment, a natural crab shell was used as a raw material to prepare the HA/CS composite coating by alkali treatment and hydrothermal reaction at various temperatures. The microstructure, morphology and phase composition of the coating surfaces were analyzed by XRD, SEM, and FTIR, and the sample coated with HA/CS was soaked in simulated body fluid (SBF) to evaluate its bioactivity. The experimental results showed that the HA/CS composite coatings through hydrothermal treatment at various temperatures can be successfully fabricated on the surface of the Ti alloy. HA on the coating surface exhibited mainly spherical particles and contained A- and B-type carbonate. When the hydrothermal temperature was up to 200 °C, the spherical particles were approximately 20–40 nm. An ultrasonic vibration test was used to evaluate the adhesion of the coatings, showing that the CS exhibited significantly improved adhesion capacity to the substrate. After being soaked in SBF for 7 days, apatite was deposited on the entire surfaces of the HA/CS coatings, indicating that the coating possesses excellent bioactivity.

Keywords: bioactivity; chitosan; composite coating; hydrothermal treatment; hydroxyapatite; titanium alloy



Citation: Hsu, H.-C.; Wu, S.-C.; Lin, C.-Y.; Ho, W.-F. Characterization of Hydroxyapatite/Chitosan Composite Coating Obtained from Crab Shells on Low-Modulus Ti–25Nb–8Sn Alloy through Hydrothermal Treatment. *Coatings* **2023**, *13*, 228. <https://doi.org/10.3390/coatings13020228>

Academic Editor: Liviu Duta

Received: 30 December 2022

Revised: 15 January 2023

Accepted: 17 January 2023

Published: 18 January 2023



Copyright: © 2023 by the authors. Licensee MDPI, Basel, Switzerland. This article is an open access article distributed under the terms and conditions of the Creative Commons Attribution (CC BY) license (<https://creativecommons.org/licenses/by/4.0/>).

1. Introduction

Because titanium (Ti) alloys have good biocompatibility, appropriate mechanical properties, and excellent corrosion resistance, they are widely used as a biomedical implants [1–4]. Ti has excellent biocompatibility because it readily reacts with oxygen in the air to form a dense oxide layer (TiO₂) on the surface. Additionally, the oxide layer can retard the release of metal ions, reducing the harm to humans [2]. Although Ti alloys exhibit many excellent properties, they are inherently bioinert and do not bond well to bone. In order to ameliorate this problem, bioactive coatings, such as hydroxyapatite (HA), bioglass, and titania, are usually made on Ti surfaces. HA has been widely used as a coating layer [5], and it is the main mineral component of the human skeleton, with excellent biocompatibility, biological activity, osseointegration and non-toxicity [6,7]. The adhesion of the coating to the substrate is an important issue that affects the long-term stability of the implant. Due to the mismatch of the thermal expansion coefficient between ceramic coating and metal substrate, residual stress was induced, which causes the coating to peel off easily [8–11].

Some literature indicated that the interfacial bonding can be improved by adding polymers to the coatings, such as chitosan (CS), collagen, gelatin and polylactide [12–15].

CS is a natural polysaccharide polymer, similar in structure to glucosamine and collagen, which can be easily derived from chitin by N-deacetylation with hot alkali. CS is currently used as dermal regeneration templates, hemostatic agents and drug delivery systems [16–18]. In addition, CS is widely used in biomedical materials because it is a non-toxic biopolymer and shows highly hydrophilic and good antibacterial properties. The antibacterial activity of CS comes from the electrostatic interaction. The amino group of CS is positively charged and interacts with the negatively charged microbial cell membrane, resulting in the leakage of bacterial intracellular components, thus making CS have good antibacterial properties [19–21].

Recently, HA/CS composites are often used as scaffolds, dressings, and coatings for implants. Jugowiec et al. [11] prepared nano-HA/CS by electrophoretic deposition on the surface of Ti–13Nb–13Zr alloy. The experimental results showed that the composite coating had better adhesion with the Ti alloy substrate and can improve the corrosion resistance of the Ti alloy. Pang et al. [19] fabricated HA/CS composite coatings on 316L stainless steel substrates using cathodic electrophoretic deposition. The CS with inherent binding properties plays a vital role in the good bonding between the coatings and the substrates, and the prepared composite coatings provided corrosion protection for the stainless steel substrates. Tang et al. [22] prepared carbonated HA/CS coatings on Ti–6Al–4V substrates using electrophoresis deposition. The carbonated HA/CS coatings exhibited moderately hydrophilic surfaces due to the presence of the CS. They also showed that the composite coating exhibited better cell morphology, adhesion, spreading, and proliferation compared to the carbonated HA coating.

Pure Ti and Ti–6Al–4V alloys have been widely used as biomedical materials, but they exhibit a low wear resistance, a high elastic modulus, and a low shear strength [23,24]. Therefore, many new Ti alloys have been developed in the past few decades to overcome these problems. A new Ti–25Nb–8Sn alloy developed by our research group exhibited much lower elastic modulus (52 GPa) than those of Ti–6Al–4V ELI alloy (110 GPa), Co–Cr–Mo alloy (230 GPa) and stainless steel (205 GPa) [25]. When the elastic modulus of the metal implant is much higher than that of the surrounding bone tissue, a stress shielding effect is generated, resulting in the absorption of the adjacent bone tissue and the loosening of the implant [26]. The main purpose of this study is to modify the surface of Ti–25Nb–8Sn alloy by preparing a bioactive coating. In this work, crab shells were used as raw materials to prepare the composite coating of HA/CS on the Ti–25Nb–8Sn alloy surface by hydrothermal method. A general approach is to prepare the raw materials of the coating by adding CS and HA separately, but the present experiment simultaneously synthesized HA and CS directly from the crab shell. Additionally, the HA and CS are obtained from crab shells in this work, which is different from the use of chemical agents in most literature. The hypothesis of this study is that CS can act as a bonding layer between the substrate and the composite coating. This study investigated the effects of hydrothermal temperatures on the features of the HA/CS coatings, including their morphology, microstructure, and phase composition. Additionally, the adhesion between the coating and the substrate was assessed, and in vitro bioactivity assay was evaluated. The bioactivity referred to in this study means that the material is capable of forming hydroxyl apatite minerals on its surface in artificially simulated body fluid (SBF) [27].

2. Materials and Methods

The Ti–25Nb–8Sn alloy used in this experiment was made of Ti sheet (99.7% in purity, thickness 0.5 mm), niobium wire (99.95% in purity, diameter 0.5 mm) and tin wire (99.95% in purity, diameter 1 mm) by using arc melting and a vacuum pressurized casting system under argon atmosphere. All the metals were purchased from Ultimate Materials Technology Co., Ltd., Hsinchu, Taiwan. High-purity argon (99.999%) was used as a protective atmosphere and adjusted to the appropriate pressure. The oxide layers on the ingots were

removed using an electric dental handpiece (UM500SBT, NSK, Tokyo, Japan), and then these specimens were washed in C_2H_5OH by ultrasonic cleaning for 10 min. Melting was performed five times in a copper crucible to achieve chemical homogeneity. After the sixth melting step, the molten alloy was quickly poured into a graphite mold placed in the casting chamber. The detailed casting procedure was described previously [28].

Ti–25Nb–8Sn specimens were ground with 100-, 400-, and 600-grit sandpaper. After ultrasonic cleaning for 10 min in C_2H_5OH , the samples were subjected to alkali treatment by placing them in a 5 M NaOH solution at 60 °C for 24 h in a constant temperature water bath. The specimens were then washed twice with distilled water for 5 min each time.

Discarded mud crab shells (genus *Scylla*) were collected from local restaurants in Taiwan; 2 g of crab shell powder was added to 36.5 wt.% HCl aqueous solution, and then H_3PO_4 was added. Followed by deacetylation at 105 °C for 60 min with NaOH solution, the synthesized product was repeatedly cleaned with deionized water and then filtered by suction. The final product was dried in an oven at 45 °C for 24 h to obtain the HA/CS powder. Afterward, the above-mentioned alkali-treated Ti alloy samples were put into a Teflon jar with HA/CS solution containing 1.5 g of HA/CS powder, 50 mL of deionized water, and 10 mL of CH_3COOH . The lid of the Teflon jar was locked, followed by placing it into an autoclave for a hydrothermal reaction. The hydrothermal temperatures were set to 100, 125, 150, 175, or 200 °C, and the holding time was 24 h. Finally, the HA/CS-coated Ti alloy was washed with deionized water and placed in a 45 °C oven for 24 h.

To assess the effect of CS on the adhesion of the coating to the substrate, a qualitative measure was performed using an ultrasonic vibration test [29]. In this experiment, the HA/CS-coated sample prepared by hydrothermal treatment at 100 °C for 24 h was adopted. An HA-coated sample prepared by the same hydrothermal condition was used as a control. The samples were tested in an ultrasonic oscillator (DC200H, DELTA, New Taipei City, Taiwan) at a power of 200 W for 10 min. The surface morphology was then observed using a field emission scanning electron microscope (FE-SEM; S-4800, Hitachi, Tokyo, Japan) to understand the cohesiveness of the coating. Before and after the ultrasonic vibration test, the weights of the test samples were, respectively, measured and their weight loss was calculated.

In this study, specimens were immersed in SBF to assess their bioactivity. The samples were soaked in SBF solution at 37 °C in pH 7.4 for 1 and 7 days. After their immersion in SBF for various periods, the samples were removed and washed with deionized water, and then dried. The SBF solution has similar ionic strength values to human plasma and is based on the formulation proposed by Kokubo and Takadama [30].

The phase analyses of the surface coatings were analyzed by a high-resolution X-ray diffractometer (D8 Discover, Bruker, Berlin, Germany), using $Cu K_{\alpha}$ radiation ($\lambda = 1.5405 \text{ \AA}$) and operating at 40 kV and 40 mA. The surface morphologies of the samples were observed using a field emission scanning electron microscope (FE-SEM; S-4800, Hitachi, Tokyo, Japan) at a voltage of 10 or 15 kV. The chemical compositions of the coatings were examined using an energy dispersive spectrometer (EDS) at a voltage of 15 kV. The functional groups of the coatings were analyzed using a Fourier transform infrared spectrometer (FTIR; Cary 630, Agilent, Santa Clara, CA, USA).

3. Results

3.1. Morphology of HA/CS Composite Coatings

The FE-SEM images of the coating surfaces of Ti–25Nb–8Sn alloy prepared by alkali treatment and hydrothermal reaction under various hydrothermal temperatures for 24 h are shown in Figure 1. The low-magnification images of Figure 1a–e showed that the surfaces of all the HA/CS coatings were flat and free of cracks. When the hydrothermal temperatures were 125 and 175 °C, some areas with larger agglomerated HA particles can be observed. From the high-magnification SEM photos of Figure 1f–j, it was clearly observed that the entire surfaces of the composite coatings were covered by spherical HA

particles. Below 150 °C, the size of HA particles was approximately 5–10 nm; however, it was increased to 20–40 nm when the reaction temperature rose to 200 °C.

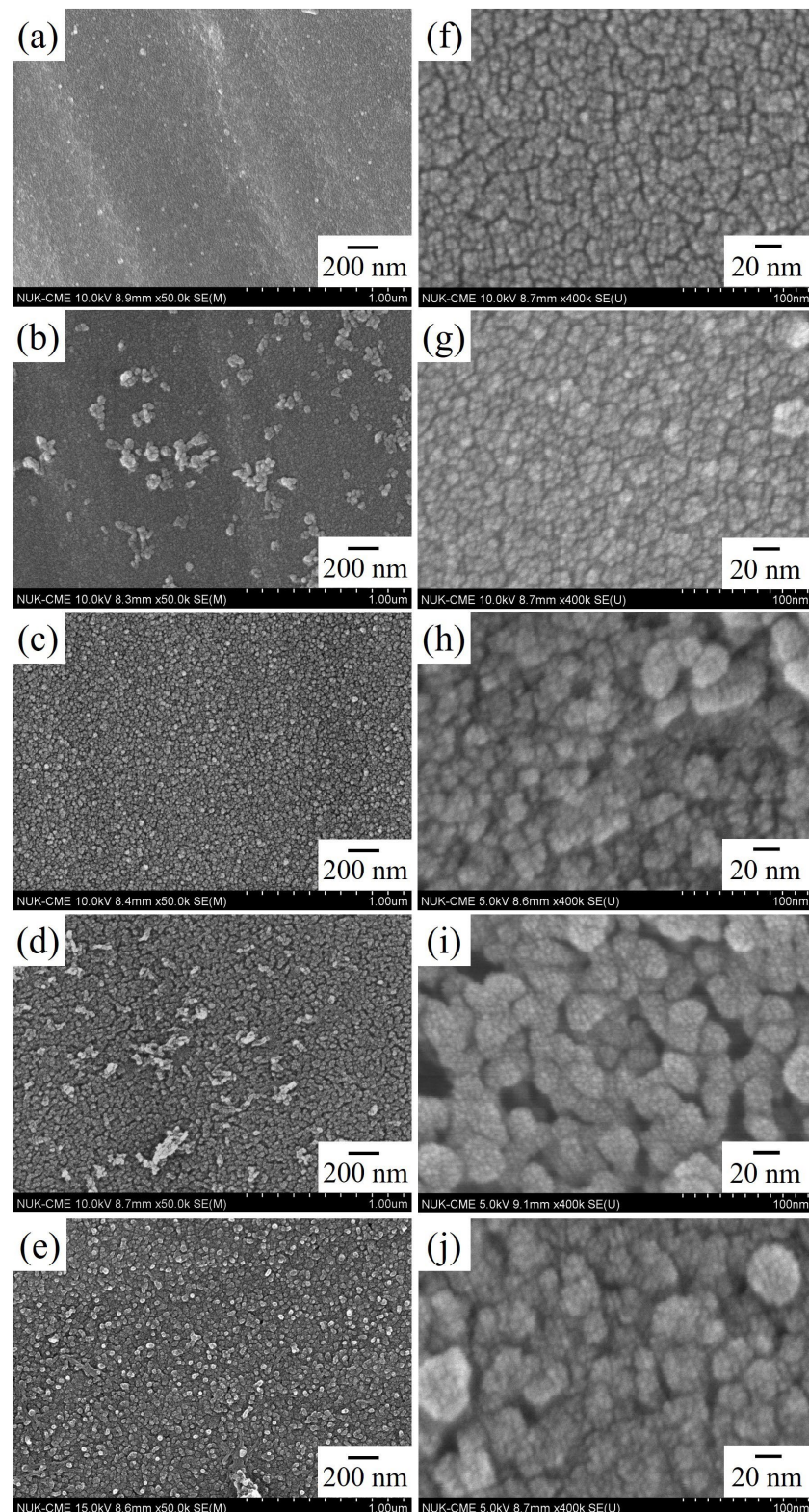


Figure 1. FE-SEM images of the coating surfaces of Ti-25Nb-8Sn alloy prepared by alkali treatment and hydrothermal reaction under various hydrothermal temperatures for 24 h. (a,f) 100 °C; (b,g) 125 °C; (c,h) 150 °C; (d,i) 175 °C; (e,j) 200 °C.

Figure 2 is the FE-SEM images of a HA/CS composite coating prepared under the hydrothermal temperature of 200 °C after scratching with a diamond blade. Since the surface coatings of the samples prepared at various hydrothermal temperatures had similar results, post-scratch photos only for the sample taken at 200 °C were provided. It is observed from the FE-SEM image at low magnification (Figure 2a) that the CS was well attached to the surface of the alloy substrate, and the HA layer was located above the CS coating. The high-magnification SEM image of the scratched coating surface (Figure 2b) showed that the CS was draped over the surface of the Ti substrate, which was attributed to the excellent binding and film-forming property of the CS [31].

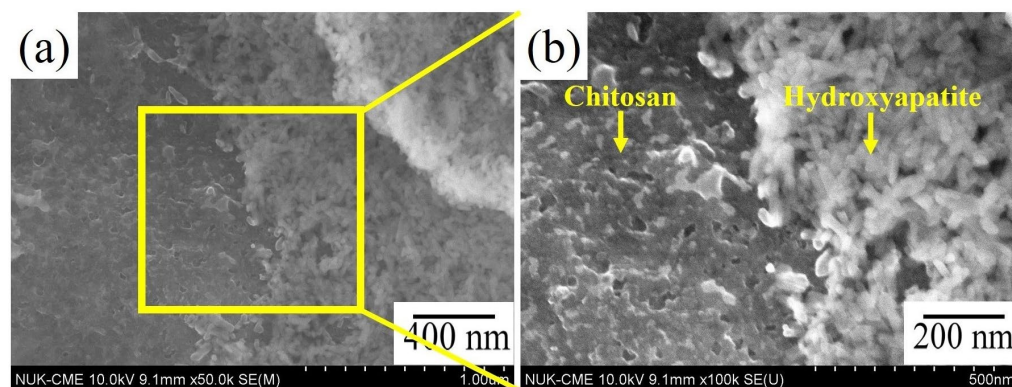


Figure 2. FE-SEM images of a HA/CS composite coating on Ti-25Nb-8Sn alloy prepared under the hydrothermal temperature of 200 °C after scratching with a diamond blade. (a) Low magnification image; (b) high magnification image.

3.2. Structure of HA/CS Composite Coatings

Figure 3 shows the XRD patterns of HA/CS composite coatings on Ti-25Nb-8Sn alloy after alkali treatment and hydrothermal reaction at different temperatures. The diffraction peaks at 28.1°, 28.94°, 31.8°, 32.92° and 34.77° corresponded to the HA phase. At the hydrothermal temperatures of 175 and 200 °C, the diffraction peaks of sodium titanate and anatase phases became more obvious, mainly formed from alkali treatment [32]. The diffraction peaks of CS were weaker and broader, mainly due to the fact that the CS belongs to an amorphous-crystalline polymer [13,22,33]. The diffraction peaks of HA were also much weaker and broader, which may be related to the thinner HA coating and the nanometer size of the crystals [9,12,13]. Additionally, Xue et al. [34] indicated that the broadening of the diffraction peaks of the HA may be due to the substitution of carbonate ions. In the current study, the HA contained carbonate ions and the result will be discussed later in the FTIR section.

Figure 4 shows the FTIR spectra of HA/CS coatings on Ti-25Nb-8Sn alloy after alkali treatment and hydrothermal reaction at different temperatures. The results showed that the band at 1653 cm^{-1} was for amide I (C=O), the bands at 1552, 1589, 1600, and 1658 cm^{-1} were assigned to amide II (N-H), and the band at 1293 cm^{-1} corresponded to amide III (-CN). The C-O group appeared at 1031 cm^{-1} . All of these bands were characteristic peaks of CS. The main functional groups of the HA are PO_4^{3-} at 665, 974, 1014, 1034 cm^{-1} and OH^- at 1700–1900 and 3600–3900 cm^{-1} . The band located at 1406, 1426 cm^{-1} was attributed to B-type carbonate-containing HA (replacement of PO_4^{3-} groups by CO_3^{2-} groups). On the other hand, A-type carbonate-containing HA (replacement of OH^- groups by CO_3^{2-} groups) was characterized by peaks at 1465 and 1500 cm^{-1} [35].

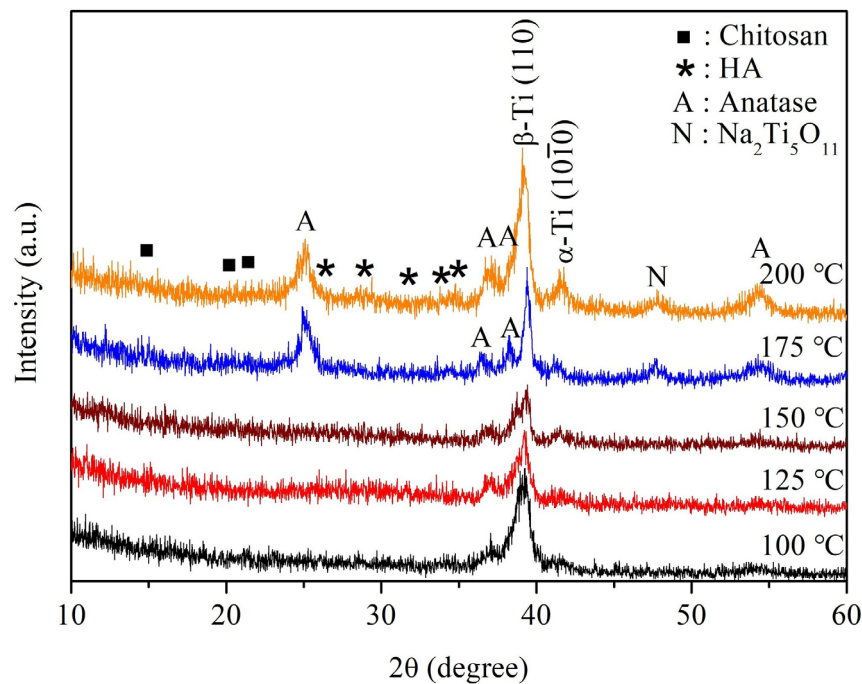


Figure 3. XRD patterns of HA/CS composite coatings on Ti-25Nb-8Sn alloy after alkali treatment and hydrothermal reaction at various temperatures.

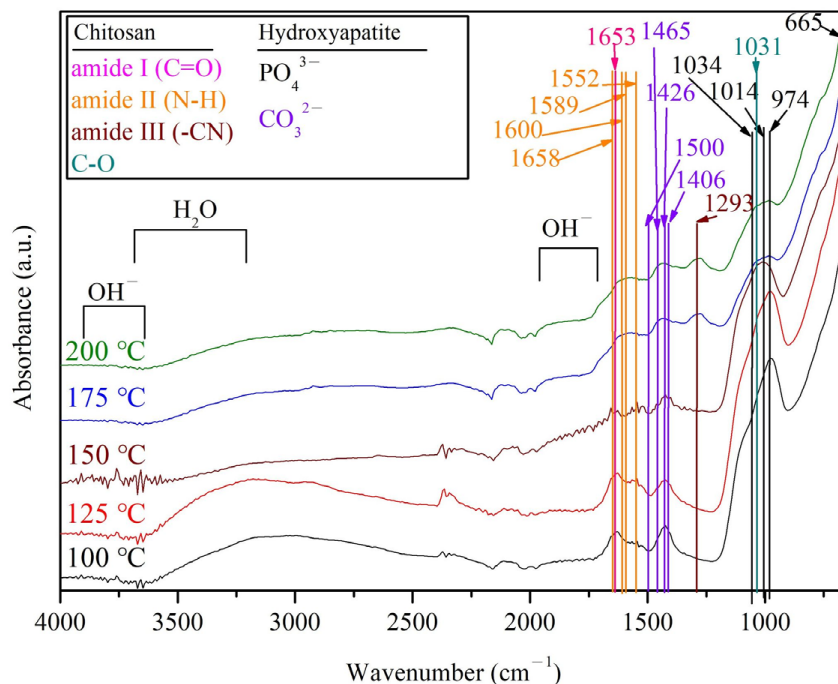


Figure 4. FTIR spectra of HA/CS composite coatings on Ti-25Nb-8Sn alloy after alkali treatment and hydrothermal reaction at various temperatures.

3.3. Adhesion of HA/CS Composite Coatings

Figure 5 is SEM images of the coating surfaces before and after ultrasonic cleaning for 10 min, and both the pure HA coating and the HA/CS composite coating prepared by hydrothermal treatment at 100 °C for 24 h were examined here. The results showed that the HA coating composed of single-phase HA (Figure 5b) was significantly peeled off when compared to the HA/CS composite coating (Figure 5d). Figure 6 shows the weight reductions in both the HA coating and the HA/CS composite coating after ultrasonic

vibration for 10 min. The weight loss of the HA coating was about 20%, while that of the HA/CS composite coating was only approximately 0.05%. Additionally, at 125 and 175 °C, the samples had relatively smaller weight loss, which may be related to the larger agglomerated HA particles on the coatings under these temperatures.

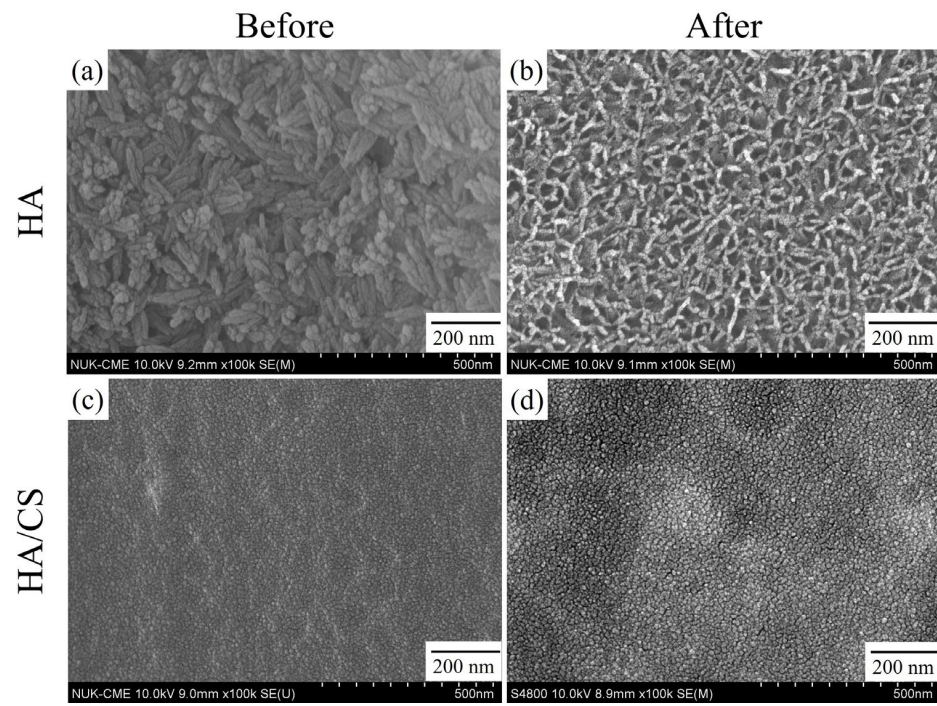


Figure 5. SEM images of coating surfaces before and after ultrasonic cleaning for 10 min, and both pure HA coating and HA/CS composite coating prepared by hydrothermal treatment at 100 °C for 24 h. (a) HA coating surface before ultrasonic cleaning; (b) HA coating surface after ultrasonic cleaning; (c) HA/CS coating surface before ultrasonic cleaning; (d) HA/CS coating surface after ultrasonic cleaning.

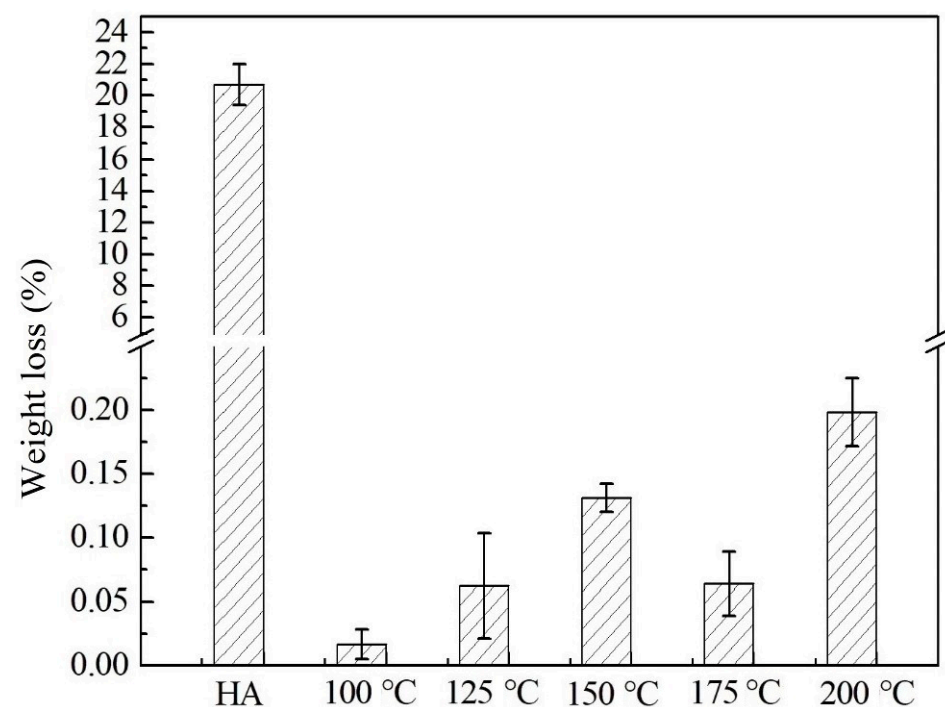


Figure 6. Weight reductions of both pure HA coating and HA/CS composite coating after ultrasonic cleaning for 10 min.

3.4. Characterization of HA/CS Composite Coating

In this study, Kokubo's solution (SBF solution) proposed by Kokubo and Takadama [30] was used for *in vitro* bioactivity assay. Figure 7 is the FE-SEM photos of the HA/CS coating surfaces, which were subjected to alkali treatment and hydrothermal reaction at different temperatures, and immersed in SBF for 1 day and 7 days. After soaking in SBF for 1 day, all the specimens had spherical apatite deposits on the surfaces, although the original coatings were still observed on the surfaces of the samples prepared by hydrothermal treatment. As the immersion time was prolonged to 7 days, all the specimen surfaces were covered with a large number of apatite precipitates. Thus, the result indicates that the HA/CS composite coatings hydrothermally synthesized in the present study have good bioactivity.

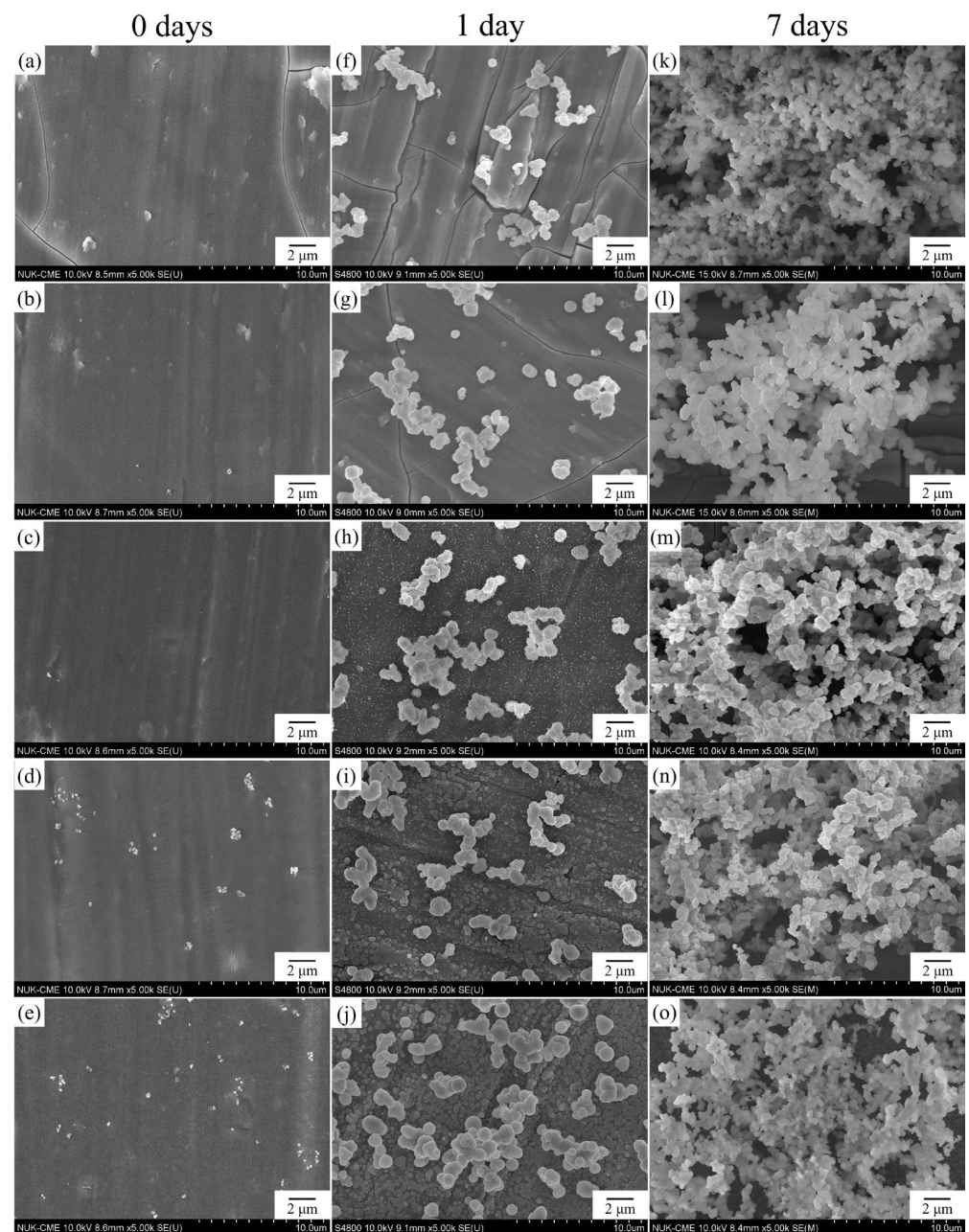


Figure 7. FE-SEM photos of HA/CS coating surfaces subjected to alkali treatment and hydrothermal reaction at various temperatures after immersion in SBF for 1 day and 7 days. (a,f,k) 100 °C; (b,g,l) 125 °C; (c,h,m) 150 °C; (d,i,n) 175 °C; (e,j,o) 200 °C.

Figure 8 is FTIR spectra of HA/CS coatings on the surfaces of Ti-25Nb-8Sn alloy after alkali treatment and hydrothermal reaction at various temperatures, followed by soaking in SBF for 7 days. The major stretching vibration of carbonate groups (CO_3^{2-}) appeared at 1418, 1462, and 1535 cm^{-1} . The samples treated at hydrothermal temperatures of 175 and 200 $^\circ\text{C}$ showed a significantly higher intensity of CO_3^{2-} bands located in the range of 2000–2300 cm^{-1} , resulting from more apatite deposition after soaking in SBF.

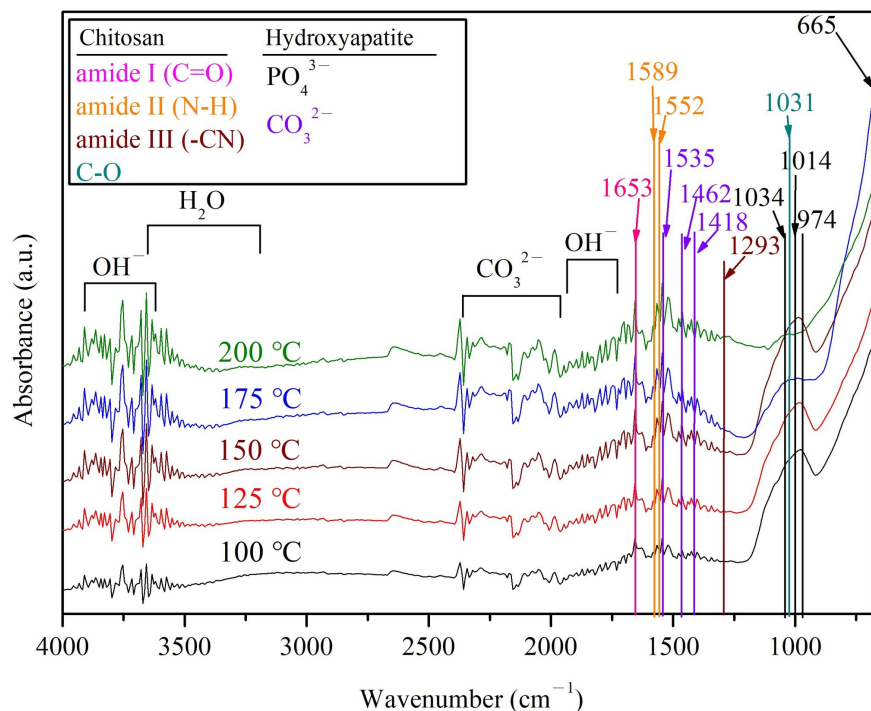
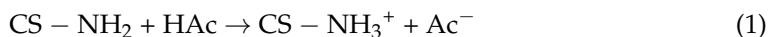


Figure 8. FTIR spectra of HA/CS composite coatings on Ti-25Nb-8Sn alloy after alkali treatment and hydrothermal reaction at various temperatures after soaking in SBF for 7 days.

4. Discussion

As shown in Figure 2, a large number of rod-shaped HA particles dispersed uniformly in the CS matrix. The rod-like HA particles had a diameter of 30–50 nm and a length of 40–60 nm. Pang et al. [19] prepared HA/CS composite coatings on 316L stainless steel substrates by electrophoretic deposition, which had similar morphologies of HA particles and CS layer to that in the present work. When adding 8.0 g/L HA into 0.5 g/L CS solution, the morphology of the HA nanoparticles was observed to be agglomerated with rod-like crystals.

In this study, CS becomes a cationic polyelectrolyte after dissolving CS in CH_3COOH (HAc) through the following equation [36,37]:



Abundant hydroxyl ion (OH^-) groups were formed on the surface of NaOH-treated Ti-25Nb-8Sn through the Na^+ and H_3O^+ ion exchange [38]. The surface OH^- groups induced a neutralization of the positively charged CS macromolecules and the formation of an insoluble CS deposit on the Ti substrate:



Additionally, the HA nanoparticles were positively charged due to the CS absorbed by the HA nanoparticles [19]. Because the velocity of migration of positively charged HA/CS was slower than that of the positively charged CS, the CS layer was precipitated

preferentially on the surface of the Ti substrate. It is worth noting that the CS coating has good adhesion to stainless steel, Ti and other substrates [19,31,36].

In this work, AB-type carbonate-containing HA was prepared in the HA/CS coatings (Figure 4). The incorporation of carbonate into HA can cause a change in the crystal structure and result in a decrease in crystallinity and an increase in solubility, which led to an increase in local concentrations of calcium and phosphorus ions that are necessary for new bone formation. Therefore, carbonate-substituted HA has better biological activity [39].

The CS exhibited significantly improved adhesion capacity to the substrate (Figures 5 and 6). Moskalewicz et al. [16] produced the HA/CS composite coating on Ti-6Al-7Nb alloy substrate by electrophoretic deposition. They asserted that the good adhesion of this coating to the substrate is mainly due to the CS matrix, which has a structure similar to that of glycosaminoglycan and can favor the bonding between the coating and the Ti substrate.

Tiyyagura et al. [40] examined the surfaces of CS coating on the porous magnesium monoliths after soaking in SBF. They found that the dominant presence of CO_3^{2-} bands ($2000\text{--}2300\text{ cm}^{-1}$) was due to the obvious apatite deposition, which is in agreement with the results in the present study (Figure 8). In addition, the specimens prepared by hydrothermal temperatures of 175 and 200 °C showed a significant low-intensity PO_4^{3-} band at $1000\text{--}1100\text{ cm}^{-1}$ (Figure 8), possibly with thicker carbonate layers (B-type carbonate) or amorphous apatite [40]. Therefore, in the present study the samples prepared by hydrothermal reaction at 175 and 200 °C exhibited faster apatite formation capability, i.e., superior bioactivity.

In this study, alkali treatment and hydrothermal reaction were used to modify the surface of Ti alloy with bioactivity, which is characterized by simplicity and industrial applicability. Nevertheless, the thickness control of the coating needs to be further optimized through hydrothermal parameters. In this experiment, crab shells were used to directly synthesize HA and CS, which is different from the method of adding CS and HA, respectively, adopted in most literature [19,22,41]. However, the main limitation of this technique may lie in the degradability of biomass materials, especially CS. Therefore, the adhesion between the coating and the substrate may deteriorate, causing the implant to fail.

Biomaterial surface properties can regulate cellular responses and affect implant osseointegration [42]. It is recommended that further studies include surface energy, topography, wettability, cellular testing, and animal testing.

5. Conclusions

The main purpose of this study is to prepare bioactive coating on the surface of Ti-25Nb-8Sn alloy with low elastic modulus by using crab shells as a raw material. FE-SEM images showed that larger agglomeration of HA particles on the coating surfaces was clearly observed at hydrothermal temperatures of 125 and 175 °C. When the temperature was below 150 °C, the size of the spherical HA particles was about 5–10 nm. As the temperature rose up to 200 °C, the size of the particles became 20–40 nm. HR-XRD analyses showed that sodium titanate, anatase, CS and HA were found on the surface of the Ti alloy. FTIR analyses presented that the main functional groups of CS were amide I (C=O), amide II (N-H) and amide III (-CN). The functional groups of HA were mainly PO_4^{3-} , OH^- , and CO_3^{2-} . Ultrasonic vibration test indicated that the peeling off of the single-phase HA coating was observed obviously. By contrast, the HA/CS composite coating exhibited better adhesion. The SBF immersion test demonstrated that the HA/CS composite coating had good bioactivity. Additionally, the samples prepared by hydrothermal reactions at 175 and 200 °C exhibited faster apatite formation capability.

Author Contributions: Conceptualization, H.-C.H., C.-Y.L. and W.-F.H.; methodology, H.-C.H., S.-C.W., C.-Y.L. and W.-F.H.; validation, H.-C.H. and W.-F.H.; formal analysis, C.-Y.L. and W.-F.H.; investigation, C.-Y.L. and W.-F.H.; resources, H.-C.H., S.-C.W. and W.-F.H.; data curation, H.-C.H., S.-C.W. and C.-Y.L.; writing and original draft preparation, C.-Y.L. and W.-F.H.; supervision and

writing—review and editing, H.-C.H. and W.-F.H. All authors have read and agreed to the published version of the manuscript.

Funding: This research was funded partially by National University of Kaohsiung.

Institutional Review Board Statement: Not applicable.

Informed Consent Statement: Not applicable.

Data Availability Statement: Not applicable.

Acknowledgments: The authors acknowledge the partial financial support of National University of Kaohsiung.

Conflicts of Interest: The authors declare no conflict of interest.

References

1. Arias-González, F.; Rodríguez-Contreras, A.; Punset, M.; Manero, J.M.; Barro, Ó.; Fernández-Arias, M.; Lusquiños, F.; Gil, J.; Pou, J. Laser-Deposited Beta Type Ti-42Nb Alloy with Anisotropic Mechanical Properties for Pioneering Biomedical Implants with a Very Low Elastic Modulus. *Materials* **2022**, *15*, 7172. [[CrossRef](#)] [[PubMed](#)]
2. Bocchetta, P.; Chen, L.-Y.; Tardelli, J.D.C.; Reis, A.C.d.; Almeraya-Calderón, F.; Leo, P. Passive Layers and Corrosion Resistance of Biomedical Ti-6Al-4V and β -Ti Alloys. *Coatings* **2021**, *11*, 487. [[CrossRef](#)]
3. Asri, R.I.M.; Harun, W.S.W.; Samykano, M.; Lah, N.A.C.; Ghani, S.A.C.; Tarlochan, F.; Raza, M.R. Corrosion and surface modification on biocompatible metals: A review. *Mater. Sci. Eng. C* **2017**, *77*, 1261–1274. [[CrossRef](#)] [[PubMed](#)]
4. Sarraf, M.; Ghomi, E.R.; Alipour, S.; Ramakrishna, S.; Sukiman, N.L. A state-of-the-art review of the fabrication and characteristics of titanium and its alloys for biomedical applications. *Bio-Des. Manuf.* **2022**, *5*, 371–395. [[CrossRef](#)] [[PubMed](#)]
5. Schwartz, A.; Kossenko, A.; Zinigrad, M.; Gofer, Y.; Borodianskiy, K.; Sobolev, A. Hydroxyapatite Coating on Ti-6Al-7Nb Alloy by Plasma Electrolytic Oxidation in Salt-Based Electrolyte. *Materials* **2022**, *15*, 7374. [[CrossRef](#)]
6. Almulhim, K.S.; Syed, M.R.; Alqahtani, N.; Alamoudi, M.; Khan, M.; Ahmed, S.Z.; Khan, A.S. Bioactive Inorganic Materials for Dental Applications: A Narrative Review. *Materials* **2022**, *15*, 6864. [[CrossRef](#)]
7. Harun, W.S.W.; Asri, R.I.M.; Alias, J.; Zulkifli, F.H.; Kadirgama, K.; Ghani, S.A.C.; Shariffuddin, J.H.M. A comprehensive review of hydroxyapatite-based coatings adhesion on metallic biomaterials. *Ceram. Int.* **2018**, *44*, 1250–1268. [[CrossRef](#)]
8. Jagadeeshanayaka, N.; Awasthi, S.; Jambagi, S.C.; Srivastava, C. Bioactive surface modifications through thermally sprayed hydroxyapatite composite coatings: A review of selective reinforcements. *Biomater. Sci.* **2022**, *10*, 2484–2523. [[CrossRef](#)]
9. He, Y.; Zhang, Y.; Zhang, J.; Jiang, Y.; Zhou, R. Fabrication and characterization of Ti-13Nb-13Zr alloy with radial porous Ti-HA coatings for bone implants. *Mater. Lett.* **2017**, *209*, 543–546. [[CrossRef](#)]
10. Rajesh, K.; Ghosh, S.; Islam, A.; Rangaswamy, M.K.; Haldar, S.; Roy, P.; Keshri, A.K.; Lahiri, D. Multilayered porous hydroxyapatite coating on Ti6Al4V implant with enhanced drug delivery and antimicrobial properties. *J. Drug Deliv. Sci. Technol.* **2022**, *70*, 103155. [[CrossRef](#)]
11. Jugowiec, D.; Lukaszczyk, A.; Cieniek, L.; Kowalski, K.; Rumian, L.; Pietryga, K.; Kot, M.; Pamula, E.; Moskalewicz, T. Influence of the electrophoretic deposition route on the microstructure and properties of nano-hydroxyapatite/chitosan coatings on the Ti-13Nb-13Zr alloy. *Surf. Coat. Technol.* **2017**, *324*, 64–79. [[CrossRef](#)]
12. Atak, B.H.; Buyuk, B.; Huysal, M.; Isik, S.; Senel, M.; Metzger, W.; Cetin, G. Preparation and characterization of amine functional nano-hydroxyapatite/chitosan bionanocomposite for bone tissue engineering applications. *Carbohydr. Polym.* **2017**, *164*, 200–213. [[CrossRef](#)] [[PubMed](#)]
13. Hahn, B.D.; Park, D.S.; Choi, J.J.; Ryu, J.H.; Yoon, W.H.; Choi, J.H.; Kim, H.E.; Kim, S.G. Aerosol deposition of hydroxyapatite-chitosan composite coatings on biodegradable magnesium alloy. *Surf. Coat. Technol.* **2011**, *205*, 3112–3118. [[CrossRef](#)]
14. Kang, S.; Haider, A.; Gupta, K.C.; Kim, H.; Kang, I. Chemical Bonding of Biomolecules to the Surface of Nano-Hydroxyapatite to Enhance Its Bioactivity. *Coatings* **2022**, *12*, 999. [[CrossRef](#)]
15. Sharma, S.; Gupta, V.; Mudgal, D. Current trends, applications, and challenges of coatings on additive manufacturing based biopolymers: A state of art review. *Polym. Compos.* **2022**, *43*, 6749–6781. [[CrossRef](#)]
16. Moskalewicz, T.; Kot, M.; Seuss, S.; Kedzierska, A.; Czyrska-Filemonowicz, A.; Boccaccini, A.R. Electrophoretic deposition and characterization of HA/Chitosan nanocomposite coatings on Ti6Al7Nb alloy. *Met. Mater. Int.* **2015**, *21*, 96–103. [[CrossRef](#)]
17. Lu, X.; Li, X.; Yu, J.; Ding, B. Nanofibrous hemostatic materials: Structural design, fabrication methods, and hemostatic mechanisms. *Acta Biomater.* **2022**, *154*, 49–62. [[CrossRef](#)]
18. Bashir, S.M.; Ahmed Rather, G.; Patricio, A.; Haq, Z.; Sheikh, A.A.; Shah, M.Z.u.H.; Singh, H.; Khan, A.A.; Imtiyaz, S.; Ahmad, S.B.; et al. Chitosan Nanoparticles: A Versatile Platform for Biomedical Applications. *Materials* **2022**, *15*, 6521. [[CrossRef](#)]
19. Pang, X.; Zhitomirsky, I. Electrophoretic deposition of composite hydroxyapatite-chitosan coatings. *Mater. Charact.* **2007**, *58*, 339–348. [[CrossRef](#)]
20. Atay, H.Y.; Celik, E. Investigations of antibacterial activity of chitosan in the polymeric composite coatings. *Prog. Org. Coat.* **2017**, *102*, 194–200. [[CrossRef](#)]

21. Li, J.; Fu, J.; Tian, X.; Hua, T.; Poon, T.; Koo, M.; Chan, W. Characteristics of chitosan fiber and their effects towards improvement of antibacterial activity. *Carbohydr. Polym.* **2022**, *280*, 119031. [[CrossRef](#)] [[PubMed](#)]
22. Tang, S.; Tian, B.; Guo, Y.J.; Zhu, Z.A.; Guo, Y.P. Chitosan/carbonated hydroxyapatite composite coatings: Fabrication, structure and biocompatibility. *Surf. Coat. Technol.* **2014**, *251*, 210–216. [[CrossRef](#)]
23. Bălțatu, M.S.; Vizureanu, P.; Bălan, T.; Lohan, M.; Țugui, C.A. Preliminary Tests for Ti-Mo-Zr-Ta Alloys as Potential Biomaterials. *IOP Conf. Ser. Mater. Sci. Eng.* **2018**, *374*, 012023. [[CrossRef](#)]
24. Baltatu, I.; Sandu, A.V.; Vlad, M.D.; Spataru, M.C.; Vizureanu, P.; Baltatu, M.S. Mechanical Characterization and In Vitro Assay of Biocompatible Titanium Alloys. *Micromachines* **2022**, *13*, 430. [[CrossRef](#)] [[PubMed](#)]
25. Hsu, H.C.; Wu, S.C.; Hsu, S.K.; Syu, J.Y.; Ho, W.F. The structure and mechanical properties of as-cast Ti-25Nb-xSn alloys for biomedical applications. *Mater. Sci. Eng. A* **2013**, *568*, 1–7. [[CrossRef](#)]
26. Al Zoubi, N.F.; Tarlochan, F.; Mehboob, H.; Jarrar, F. Design of Titanium Alloy Femoral Stem Cellular Structure for Stress Shielding and Stem Stability: Computational Analysis. *Appl. Sci.* **2022**, *12*, 1548. [[CrossRef](#)]
27. Darvell, B.W. Bioactivity—Symphony or Cacophony? A Personal View of a Tangled Field. *Prosthesis* **2021**, *3*, 75–84. [[CrossRef](#)]
28. Wong, K.-K.; Hsu, H.-C.; Wu, S.-C.; Hung, T.-L.; Ho, W.-F. Structure, Properties, and Corrosion Behavior of Ti-Rich TiZrNbTa Medium-Entropy Alloys with $\beta+\alpha''+\alpha'$ for Biomedical Application. *Materials* **2022**, *15*, 7953. [[CrossRef](#)]
29. Yu, H.N.; Hsu, H.C.; Wu, S.C.; Hsu, C.W.; Hsu, S.K.; Ho, W.F. Characterization of Nano-Scale Hydroxyapatite Coating Synthesized from Eggshells Through Hydrothermal Reaction on Commercially Pure Titanium. *Coatings* **2020**, *10*, 112. [[CrossRef](#)]
30. Kokubo, T.; Takadama, H. How useful is SBF in predicting in vivo bone bioactivity? *Biomaterials* **2006**, *27*, 2907–2915. [[CrossRef](#)]
31. Sun, F.; Pang, X.; Zhitomirsky, I. Electrophoretic deposition of composite hydroxyapatite-chitosan-heparin coatings. *J. Mater. Process. Technol.* **2009**, *209*, 1597–1606. [[CrossRef](#)]
32. Kim, H.M.; Miyaji, F.; Kokubo, T.; Nakamura, T. Preparation of bioactive Ti and its alloys via simple chemical surface treatment. *J. Biomed. Mater. Res. A* **1996**, *32*, 409–417. [[CrossRef](#)]
33. Sadiq, N.M.; Aziz, S.B.; Kadir, M.F.Z. Development of Flexible Plasticized Ion Conducting Polymer Blend Electrolytes Based on Polyvinyl Alcohol (PVA): Chitosan (CS) with High Ion Transport Parameters Close to Gel Based Electrolytes. *Gels* **2022**, *8*, 153. [[CrossRef](#)]
34. Xue, C.B.; Chen, Y.Z.; Huang, Y.Z.; Zhu, P.Z. Hydrothermal synthesis and biocompatibility study of highly crystalline carbonated hydroxyapatite nanorods. *Nanoscale Res. Lett.* **2015**, *10*, 316. [[CrossRef](#)]
35. Jokanovic, V.; Jokanovic, B.; Markovic, D.; Zivojinovic, V.; Pasalic, S.; Izvonar, D.; Plavsic, M. Kinetics and sintering mechanisms of hydro-thermally obtained hydroxyapatite. *Mater. Chem. Phys.* **2008**, *111*, 180–185. [[CrossRef](#)]
36. Pang, X.; Zhitomirsky, I. Electrodeposition of composite hydroxyapatite-chitosan films. *Mater. Chem. Phys.* **2005**, *94*, 245–251. [[CrossRef](#)]
37. Fu, X.; Chang, X.; Ding, Z.; Xu, H.; Kong, H.; Chen, F.; Wang, R.; Shan, Y.; Ding, S. Fabrication and Characterization of Eco-Friendly Polyelectrolyte Bilayer Films Based on Chitosan and Different Types of Edible Citrus Pectin. *Foods* **2022**, *11*, 3536. [[CrossRef](#)]
38. Ho, W.F.; Lai, C.H.; Hsu, H.C.; Wu, S.C. Surface modification of a low-modulus Ti-7.5Mo alloy treated with aqueous NaOH. *Surf. Coat. Technol.* **2009**, *203*, 3142–3150. [[CrossRef](#)]
39. Safarzadeh, M.; Chee, C.F.; Ramesh, S. Effect of carbonate content on the in vitro bioactivity of carbonated hydroxyapatite. *Ceram. Int.* **2022**, *48*, 18174–18179. [[CrossRef](#)]
40. Tiyyagura, H.R.; Rudolf, R.; Gorgieva, S.; Fuchs-Godec, R.; Boyapati, V.R.; Mantravadi, K.M.; Kokol, V. The chitosan coating and processing effect on the physiological corrosion behaviour of porous magnesium monoliths. *Prog. Org. Coat.* **2016**, *99*, 147–156. [[CrossRef](#)]
41. Song, L.; Gan, L.; Xiao, Y.F.; Wu, Y.; Wu, F.; Gu, Z.W. Antibacterial hydroxyapatite/chitosan complex coatings with superior osteoblastic cell response. *Mater. Lett.* **2011**, *65*, 974–977. [[CrossRef](#)]
42. Rupp, F.; Liang, L.; Geis-Gerstorfer, J.; Scheideler, L.; Hüttig, F. Surface characteristics of dental implants: A review. *Dent. Mater.* **2018**, *34*, 40–57. [[CrossRef](#)] [[PubMed](#)]

Disclaimer/Publisher's Note: The statements, opinions and data contained in all publications are solely those of the individual author(s) and contributor(s) and not of MDPI and/or the editor(s). MDPI and/or the editor(s) disclaim responsibility for any injury to people or property resulting from any ideas, methods, instructions or products referred to in the content.